Diacylglycerol Kinase α regulates the formation and polarization of mature multivesicular bodies involved in the secretion of Fas ligand-containing exosomes in T lymphocytes (*).

AUTHORS: Roberto Alonso[‡**], Carla Mazzeo[¶**], Mª Carmen Rodríguez[‡], Mark Marsh[§], Alberto Fraile-Ramos[+], Víctor Calvo[¶], Antonia Avila-Flores[+], Isabel Mérida[+] and Manuel Izquierdo[¶]

[‡]Instituto de Biología y Genética Molecular (IBGM), CSIC-Universidad de Valladolid, Facultad de Medicina, Ramón y Cajal, 7, 47005 Valladolid, and [¶]Departamento de Bioquímica. Instituto de Investigaciones Biomédicas "Alberto Sols", CSIC-UAM, Facultad de Medicina, Universidad Autónoma de Madrid, c/ Arturo Duperier, 4, 28029 Madrid, Spain. [+]Centro Nacional de Biotecnología, CSIC. [§] Cell Biology Unit, MRC Laboratory for Molecular Cell Biology, University College London, Gower Street, London WC1E 6BT (UK).

Running Title: Diacylglycerol kinase α regulates exosome secretion

[**] R. Alonso and C. Mazzeo contributed equally to this article.

[¶] **Correspondence :**

Manuel Izquierdo, PhD
C-20
Instituto de Investigaciones Biomédicas "Alberto Sols"
CSIC-Universidad Autónoma de Madrid
c/Arturo Duperier, 4
28029 Madrid
SPAIN
e-mail: mizquierdo@iib.uam.es
Tel: +34 91 4973117
Fax: +34 91 5854401

* This work was supported by grants from Ministerio de Ciencia e Innovación, BFU2007-61613 and BFU2010-18726. R. Alonso was the recipient of a fellowship from the Spanish Ministerio de Ciencia y Tecnología. A. Fraile-Ramos is supported by Ramón y Cajal Program. M. Marsh is supported by the UK Medical Research Council.

Abbreviations:

Ab, antibody; AICD, Activation-induced cell death; CCh, carbamyl choline (carbachol); CTL, cytotoxic T lymphocyte; DAG, diacylclycerol; DGK, diacylglycerol kinase; ESCRT, endosomal sorting complex required for transport; FACS, fluorescence-activated cell sorter; FasL, Fas Ligand; HM1R, human muscarinic receptor, type 1; HRP, horseradish peroxidase; mAb, monoclonal antibody; ILVs, intraluminal vesicles; LBPA, lysobisphosphatidic acid; MTOC, microtubule organizing center; MVBs, multivesicular bodies; PM, plasma membrane; SEE, Staphylococcal Enterotoxin E; TCR, T-cell receptor; TGN, trans-Golgi network; WB, Western blot.

NUMBER OF WORDS: 3989 (INTRODUCTION+RESULTS+DISCUSSION)

ABSTRACT

Multivesicular bodies (MVBs) are endocytic compartments that contain intraluminal vesicles formed by inward budding from the limiting membrane of endosomes. In T lymphocytes these vesicles contain pro-apoptotic Fas ligand (FasL), that may be secreted as "lethal exosomes" upon fusion of MVBs with the plasma membrane. Diacylglycerol kinase α (DGKα) regulates the secretion of exosomes, but it is unclear how this control is mediated. T lymphocyte activation increases the number of MVBs that contain FasL. DGKα is recruited to MVBs and exosomes where it has a double function. DGKα kinase activity exerts a negative role in the formation of mature MVBs as we demonstrate by the use of an inhibitor. Downmodulation of DGKα protein resulted in inhibition of both the polarization of MVBs towards immune synapse and exosome secretion. The subcellular location of DGKα together with its complex role in the formation and polarized traffic of MVBs support the notion that DGKα is a key regulator of the polarized secretion of exosomes.

KEYWORDS: T lymphocytes/Diacylglycerol kinase α/Multivesicular bodies/Fas ligand/ exosomes/

INTRODUCTION

Exosomes are small membrane vesicles of endocytic origin that are secreted by many cells. These vesicles are formed by inward budding of the limiting membrane of late endosomes, and accumulate as intraluminal vesicles (ILVs) inside multivesicular bodies (MVBs)[1]. Stimulation of cells induces the fusion of the limiting membrane of the MVBs with the plasma membrane (PM) and the secretion of the ILVs, which then are termed exosomes[1].

Cytotoxic T lymphocytes (CTLs) use both perforin/granzyme and Fas ligand (FasL)-dependent pathways to exert their function. Regarding FasL, CTLs kill Fas^+ cells by exposing pre-formed FasL on the PM at the immunological synapse[2]. FasL induces cross-linking of the Fas death receptor on the target cell and apoptosis[3]. In CTLs, FasL is located at the limiting membrane of secretory lysosomes containing perforin/granzyme, with MVB structure[2]. Upon T cell receptor activation (TCR), MVBs undergo fusion with the PM and re-localisation of FasL to the PM occurs[2].

In addition to this transport of FasL, another mechanism for the delivery of FasL co-exists in CTLs[4]. This mechanism is due to the fact that FasL can be sorted from the limiting membrane of the MVBs to the ILVs via inward budding[4,5]. Upon cell activation, the fusion of pre-existing MVBs with the PM results in the release of exosomes containing FasL[5]. In certain cells such as Jurkat[6] or melanoma cells[7], this ILVs/MVBs pathway is the main mechanism involved in FasL traffic. Accordingly, a difference exists in FasL traffic between CTLs and non-CTLs cells as Jurkat. Although in both cell types pre-formed and activation-induced synthesis of FasL coexist, in Jurkat cells the majority of FasL undergoes sorting to the ILVs in MVBs and is secreted into exosomes[5]. In addition, no PM relocation of FasL was observed in Jurkat[5], J-HM1-2.2[8] or melanoma cells[7], even in the presence of metalloproteinase inhibitors to avoid shedding of FasL from the cell surface[9]. This supports that, in contrast to FasL found in CTLs[2], in Jurkat cells none or very little FasL is located in the limiting membrane of the MVBs.

Previous results have shown the role of diacylglycerol kinase α (DGKα), a diacylglycerol (DAG)–consuming enzyme[10], on activation[11] and activation-induced cell death (AICD) of T lymphocytes[8]. AICD was defined as an autocrine suicide triggered by T cell receptor (TCR) stimulation, which controls lymphocyte homeostasis[12], that can be mimicked by muscarinic type 1 receptor (HM1R)

stimulation with carbachol (CCh) in J-HM1-2.2 cells[13]. AICD requires *de novo* synthesis of FasL[12] and its secretion into exosomes[6,8]. Consequently, the kinetics for apoptosis initiation during AICD is slow (> 4-5 h) when compared to CTL-mediated cytotoxicity, which occurs in minutes. The inhibition of DGKα kinase activity increased the secretion of exosomes bearing FasL that was induced upon activation through TCR or the HM1R, a model for AICD[8,13]. Subsequently, the enhanced secretion of exosomes led to an increase in FasL-dependent AICD[8]. These results support that the effect of DGKα on apoptosis occurs by regulating the release of exosomes bearing *de novo* synthesized FasL[8]. However, from these studies it was not clear whether stimulation of T lymphocytes affects the traffic of MVBs. In addition, the regulatory point(s) on secretory traffic of exosomes controlled by DGKα remained obscure.

Secretory vesicular traffic involves several checkpoints controlled by DAG at which cellular stimulation and DGKα might act. These include the fission of vesicles at the *trans*-Golgi network (TGN), the generation and maturation of MVBs (i.e., number of MVBs per cell and inward vesiculation within MVB), the transport of the MVBs, and their docking and fusion to the PM[14-17]. To explore these possibilities we have used pharmacological and genetic approaches.

RESULTS

T lymphocyte activation increases the formation of mature MVBs containing FasL.

Stimulation of TCR or HM1R in J-HM1-2.2 cells induces apoptosis[13], that occurs via the release of exosomes containing CD63 and *de novo*-synthesised FasL[8]. To explore the mechanisms involved in exosome secretion, we analysed the MVB markers CD63, Lamp-1 and the lipid lysobisphosphatidic acid (LBPA) in CCh-stimulated cells. Immunofluorescence analysis of CD63, FasL and LBPA showed that these markers were located in vesicles (Fig. 1A). Comparable results were obtained in cells expressing CFP-CD63 (Fig. 1B). The stimulation enhanced the number of $CD63^+$, $FasL^+$ or $LBPA^+$ vesicles (Fig. 1A). To confirm this, a quantitative analysis was performed by flow cytometry and WB. As shown in Suppl. Fig. S1, CCh increased the fluorescence of cells stained with anti-CD63, FasL or LBPA. The subcellular fractionation on Percoll gradients has been used to analyze FasL into secretory lysosomes from CTLs[2] and MVBs from T lymphocytes[8]. The gradient from non-stimulated cells showed that $CD63^+$ and Lamp-1^+ fractions 12 and 13, which had the density of MVBs (ρ=1.05–1.06 g/ml)[8,18], contained some pre-existing FasL (Fig. 2). Stimulation with CCh for 6 hours, which up-regulate the levels of FasL mRNA[13] and protein (Suppl. Fig. S1), enhanced dramatically the amount of FasL and CD63 in the fractions corresponding to MVBs (12-13) (Fig. 2). Thus, cellular stimulation induces the recruitment of the upregulated Fas ligand to subcellular compartments migrating at the same density that MVBs

Taken together, these results may represent an increase in the formation of mature MVBs upon cell activation. To analyse this, but also to stress whether the molecules found in the same fractions were present in the MVBs, we carried out analysis of LBPA in cells expressing CFP-CD63. LBPA constitutes a bona fide marker for ILVs of mature MVBs. As shown in Fig. 1B, LBPA co-localised with CD63, and stimulation with CCh increased the number of $LBPA^+/CD63^+$ vesicles (Suppl. Fig. S2). Thus, the biochemical and immunofluorescence results, together the published results showing colocalisation of FasL with CD63 and lamp-1[5] supported that, upon CCh stimulation, there was an increase in the number of mature MVBs containing CD63, LBPA, and FasL.

To confirm these vesicles exhibited MVBs ultra-structure, we analysed cells by electron microscopy. As shown in Suppl. Fig. S3, stimulation with CCh increased the number of vesicles

containing an electron-dense content with the features of MVBs observed in CTLs[19] and T lymphocytes[5]. Taken together, the data support that stimulation of cells increased the number of mature MVBs that contain FasL. We examined next the contribution of DGKα to the biogenesis of MVBs and exosomes.

Inhibition of DGKα kinase activity increases the number of mature MVBs

Fractionation on Percoll gradients has revealed the presence of DGKα in $CD63^+$ late endosome fractions from non-stimulated cells[20]. Similar analysis following CCh treament revealed that the increase in DGKα levels in these fractions mirrored those of CD63 and FasL, suggesting that stimulation enhances the formation of DGKα-enriched MVBs (Fig. 2). We have shown that inhibition of DGKα kinase activity increased exosome release[8]. As CCh enhances association of DGKα with subcellular fractions containing MVBs, we analysed the influence of DGKα kinase activity on the formation of MVBs upon stimulation. Treatment of the cells with the inhibitor of type I DGKs R59949[21] enhanced the number of exosomes secreted in non-stimulating conditions as determined by FACS; this effect was stronger in response to CCh (from 6481 up to 9410 events) (Fig. 3A). DGKα inhibition resulted in higher levels of CD63 and its redistribution in fractions containing MVBs (Fig. 3B), and enhanced the ability of CCh to increase the number of vesicles decorated with CD63 and the number of $LBPA^+$ vesicles (Suppl. Fig. S4). The vesicles induced by CCh in the presence of R59949 displayed the features of MVBs (Suppl. Fig. S3) and contained both CFP-CD63 and LBPA (not shown). Together, these data indicate that the inhibition of DGKα kinase activity enhances the formation of $CD63^+$, $LBPA^+$ mature MVBs, which correlates with the enhanced release of exosomes.

Inactive DGKα co-localizes with MVBs

The previous experiments demonstrate that DGKα is found in subcellular fractions containing MVBs, and suggest a negative function of DGKα kinase activity in the formation of mature MVBs. If this is the case, then DGKα may be found associated with the limiting membrane of MVBs, sorted to the ILVs and then secreted in exosomes. We have demonstrated that DGKα localization is negatively regulated by its own kinase activity, since R59949 enhances association of DGKα to membranes[11]**.** Therefore, we used confocal microscopy to investigate the effect of the inhibition of DGKα kinase activity on DGKα localization. CCh in the presence of R59949 induced, in addition to the described

translocation of GFP-DGKα to the PM[11], the accumulation of GFP-DGKα in vesicles, most of them CD63+, distributed throughout the cytoplasm (Fig. 4A and 4B, arrows). Since R59949 enhanced the release of exosomes[8] and induced the formation of mature ($CD63^+$ $LBPA^+$) MVBs (Suppl. Fig. S4), we analysed by WB the exosomes secreted from cells stimulated with CCh, in the presence or the absence of R59949, for the presence of DGKα. As shown in Fig. 4C, the amount of DGKα secreted in the exosomes mirrored the increase corresponding to other proteins (i.e. CD63) or inducible FasL (compare CCh 500 vs CCh 500 plus R59949) .

Traffic of MVBs

To analyse the contribution to exosome secretion of the transport and fusion of MVBs to the PM, and to assess the effect of DGKα on these events, we analysed the traffic of MVBs. To this end, we used expression vectors for the MVB/exosome marker CD63 fused to GFP, DsRed2 or CFP. As shown in Fig. 5A, CCh enhanced the amount of GFP-$CD63^+$ and DsRed2-$CD63^+$ exosomes secreted by transfected cells, as seen with endogenous CD63 (Fig. 4C). Once the reporters were validated, we analysed the formation and traffic of MVBs containing the reporters in living cells. The expression of GFP-CD63 in non-stimulated cells revealed vesicles distributed all over the cytoplasm, and the PM was weakly stained with GFP-CD63 (Fig 5B, upper panels). Time-lapse microscopy showed a myriad of CFP-$CD63^+$ vesicles undergoing a rapid movement inside the cytoplasm (Supplementary Videos 1 and 2). Particularly upon CCh stimulation, these vesicles exhibited bidirectional motion emerging from the pericentriolar area. Stimulation with CCh for 24h increased the intensity of the labelling, the number of these granules and their dispersion within the cell (Fig. 5B, videos 1 and 2). In addition, stimulation for 6h enhanced the staining of GFP-CD63 at the PM (Fig. 5B). Some of the scattered granules appeared as ring-shaped vesicles (Supplementary video 4, zoom in Fig. 5B), brightly labelled with the chimera at the peripheral membrane. Time-lapse microscopy showed that, upon stimulation, some vesicles approached, seemed to dock to the PM and disappeared (Supplementary Videos 3, 4); these observations are compatible with the fusion of the MVBs to PM.

Next, we studied the role of DGKα pathway on the formation and fate of MVBs. R59949 enhanced the fluorescence of the intracellular vesicles and the accumulation of GFP-CD63 in the PM

upon CCh stimulation for 6 h (Fig. 5B). The CCh and R59949-induced increase in GFP-CD63 at the PM, was due to the fusion of the limiting membrane of GFP-CD63$^+$ MVBs (Videos 3 and 4). This, combined with the increased number of CD63$^+$ and LBPA$^+$ vesicles which was induced by CCh and R59949 (Figs. 1, 3, and Suppl. Figs. S2 and S4) and the enhanced secretion of GFP-CD63$^+$ exosomes (Fig. 5A), support that the inhibition of the kinase activity of DGKα increases the formation of mature MVBs containing intraluminal, CD63$^+$/LBPA$^+$ vesicles. In addition, as shown in overexposed blots (Fig. 5A), R59949 enhanced the constitutive secretion of exosomes containing GFP-CD63 as previously reported with endogenous CD63[8].

Overexpression of DGKα inhibits the formation of mature MVBs

If the effect of R59949 is exerted via the inhibition of DGKα kinase activity, it would be expected that overexpression of the enzyme would decrease the number of mature MVBs, leading to a reduction in exosome secretion[8,20]. To study the number of mature MVBs we analysed the distribution of CD63 and LBPA in cells co-transfected with CFP-CD63 and GFP-DGKα, GFP-VPS4wt, and GFP-VPS4EQ. The expression of a VPS4 ATPase-defective mutant, VPS4EQ, constitutes a control for aberrant MVBs maturation[22,23]. As shown in Fig. 6, GFP-VPS4wt was cytosolic, whereas VPS4EQ accumulated in a few, bright-fluorescent foci that co-localized with CFP-CD63 and LBPA (Fig. 6 and Suppl. Fig. S5), with the appearance of enlarged, ring-shaped vesicles. There was a reduction in the number of LBPA$^+$ vesicles in GFP-VPS4EQ$^+$ cells when compared with non-transfected cells or GFP-VPS4wt$^+$ cells (Fig. 6). CCh stimulation of non-transfected cells or GFP-VPS4wt$^+$ cells increased the number and the labelling of the LBPA$^+$ vesicles. By contrast, upon stimulation of GFP-VPS4EQ$^+$ cells, the number of LBPA$^+$ vesicles remained low and few, enlarged LBPA$^+$ vesicles were observed (Fig. 6A, 6C). The number of LBPA$^+$ vesicles was reduced in non-stimulated cells expressing GFP-DGKα (Fig. 6A); this effect was dramatic upon CCh stimulation (Fig. 6A and 6C).

With regards to the effect of DGKα on the traffic of CD63-containing vesicles, the analysis of CD63 relocation at the PM induced by CCh stimulation showed no differences between GFP-DGKα$^+$ and GFP-DGKα$^-$ cells (Fig 6B, top panels) at several time points; the same result was observed in

VPS4EQ$^+$ cells (Fig. 6B, lower panels). Thus, the expression of DGKα or VPS4EQ seemed not to affect the transport, docking and fusion of the CD63$^+$ vesicles to the PM in a non-polarized model of secretion.

The recognition of target cells by CTLs induces polarization of MVBs towards the immune synapse, and the polarized transport, docking and fusion of MVBs with the PM at the synapse[2]. Therefore, the accumulation of CD63 at the PM in a synapse model provided information to extend the findings regarding the role of DGKα on secretion to a polarized situation. To perform these experiments we used Raji cells presenting Staphylococcal Enterotoxin E (SEE) to Jurkat cells[24] expressing GFP-CD63. As seen in Suppl. Fig. S6 recorded 5 h after synapse formation, there was an accumulation of GFP-CD63$^+$ vesicles close to the synapse; the movement of vesicles in and out from this area was recorded (video 5, video 6, Suppl. Fig. S6). In addition, an accumulation of GFP-CD63 in the cell surface was observed. We verified that overexpression of DGKα inhibited, and the inhibition of DGKα increased, the secretion of exosomes in the synapse (Fig. 7), as seen in the non-polarized model (compare Fig. 7 with Figs. 4C and 5A). Subsequently, we tested that R59949 specifically reverted the inhibition on exosome secretion exerted by DGKα, but not DGKζ, since the inhibitor partially rescued the inhibitory effect of DGKα on exosome secretion, but not the corresponding to DGKζ (Fig. 7).

The absence of DGKα inhibits the polarized traffic of MVBs

Since it is possible that the absence of DGKα may exert a different effect on secretion when compared with the inhibition of the kinase activity of DGKα, we analysed polarized traffic and secretion in cells lacking DGKα. As seen in Fig. 8A, pSuper-SiRNA humanDGKα plasmid reduced the amount of DGKα protein when compared with non-relevant plasmids (Fig. 8A). This seemingly low reduction was more pronounced when DGKα was analysed in selected GFP+ cells (Fig. 9B). The interference on DGKα inhibited the polarized secretion of GFP-CD63$^+$ exosomes induced by SEE (Fig. 8B, C). We aimed to reveal traffic events underlying the effect of DGKα interference on secretion. Thus, we analysed the relocation of endogenous CD63 to the synapse, which is consequence of the degranulation of MVBs[2]. As seen in Fig. 9A, upon stimulation with SEE for 1h or 5h, the interfered GFP+ cells had low levels of cell surface CD63 when compared to GFP- cells, as assessed by flowcytometry (Fig. 9A, lower panel). The absence of DGKα did not affect the formation of mature MVBs since the number of

MVBs per cell remained unchanged (Fig. 9B). Since degranulation of MVBs was inhibited in the absence of DGKα, but both the formation of synapses and number of MVBs remained unaffected, we analysed the ability of cells DGKα$^-$ to polarize MVBs. To this end, we labelled DGKα, together with intracellular CD63 or LBPA. As seen in Fig. 9B, GFP+ cells lacking DGKα and stimulated for 1 h or 5 h were unable to polarize CD63$^+$ or LBPA$^+$ granules (not shown) towards the synapse, when compared to GFP$^-$DGKα$^+$ or GFP$^+$DGKα$^+$ cells. Therefore, most probably, an inhibition of polarization of mature MVBs towards the synapse underlied the effect of DGKα interference on secretion of exosomes.

DISCUSSION

Our data support that T lymphocyte activation increases the number of mature MVBs that contain FasL on their ILVs. Besides this effect of cell activation on formation of mature MVBs, an increase in mobilisation, docking and fusion of these MVBs to the PM may underlie the stimulated release of FasL-bearing exosomes. The inhibition of DGKα kinase activity, previously shown to enhance exosome secretion[8], also increases the formation of mature MVBs induced upon activation. However, we could not rule out a non-specific effect of the inhibitor. Thus, we tested that the inhibitor acted on DGKα, but not on DGKζ, since the inhibitor did not rescue DGKζ-induced inhibition of exosome secretion (Fig. 7). To examine a possible negative function of DGKα kinase activity in the transport, docking and fusion of MVBs with the PM, we overexpressed DGKα and analysed these events. We observed that DGKα negatively regulated the formation of mature MVBs, but did not appear to affect their subsequent traffic. In contrast, the association of DGKα with MVBs, the effect of DGKα on the formation of mature MVBs, the association of DGKα with exosomes, and its role on exosome secretion, are compatible with the idea that DGKα kinase activity is an important negative regulator of the formation of MVBs. The fact that inhibition of DGKα kinase enhances the number of mature MVBs and partially rescues the inhibition of exosome secretion conferred by DGKα overexpression, supports the notion of DGKα kinase activity act as an important negative regulator of polarized and non-polarized exosome release. In addition to the positive effect of the inhibitor on the inducible secretion, we observed also a positive effect on the constitutive secretion of exosomes (Figs. 3A and 5A)[8]. It is known that there is constitutive DAG production at intracellular membranes[25]. This DAG pool is necessary for constitutive vesicular traffic[15], and R59949 has been shown to enhance basal DAG levels on endomembranes[25], probably by inhibition of DGKs. Thus, it is conceivable that the inhibitor -by affecting intracellular DAG pools- may positively control the constitutive traffic of MVBs, and subsequently, the basal secretion of exosomes.

We investigated the role of DGKα in the polarized secretion of exosomes. By using an interference approach on a synapse model, we uncovered a positive role of DGKα on exosome secretion. In DGKα–interfered cells, polarization of MVBs and subsequent exosome release were reduced (Fig. 9). This, together with the fact that the kinase inhibitor increases polarized secretion of exosomes (Fig. 7)

implies that some non-kinase function of DGKα is required for polarized secretion. The fact that R59949 partially rescues the negative effect of DGKα overexpression on exosome secretion (Fig. 7), together the inhibitory effect that DGKα downmodulation produces on MVBs polarization and degranulation (Figs. 8, 9), suggest that different functional domains of DGKα negatively and positively control the secretory traffic of exosomes at, at least, two distinct regulatory points. Whereas the kinase domain appears to be negatively involved in formation of mature MVBs, other(s) domain(s) would be positively involved in MVBs polarization. Although both the nature of these domains and their effectors remain unknown, our results point out to a complex, fine-tuned control of the secretory traffic of exosomes exerted by DGKα.

The lipid composition of vesicles constitutes a factor in the maturation of MVBs that is susceptible to regulation by DGKα. The contribution of LBPA has interest, since LBPA provides negative curvature to the MVB limiting membrane during the inward invagination to form the ILVs[26]. In the latter study, it has been shown that ALIX, a protein that interacts with ESCRT complexes, binds to LBPA-containing liposomes. When ALIX levels were down-regulated, the formation of LBPA-containing endosomes decreased[26]. Thus, ALIX regulates the maturation of MVBs. LBPA is locally produced in MVBs[26], but the steps involved in LBPA synthesis remain unclear. Therefore, it will be interesting to analyse the consequences of the regulation of DAG levels by DGKα on both the synthesis of LBPA and the recruitment of ALIX/ESCRT to the MVBs. One possibility that may explain the inhibition of exosome secretion by DGKα and the fact that DGKα overexpression inhibits the formation of $LBPA^+$ vesicles is that the enzyme would affect the maturation (number of ILVs) of MVBs. If this is the case, then DGKα could be found associated with the MVBs and secreted in exosomes, as we have shown. Thus, quite probably, DGKα controls the inward budding in MVBs. The changes induced by R59949 in the distribution of CD63 on gradients (Fig. 3B) support this hypothesis, since the maturation of late endosomes/MVBs is associated with an increase in their content in LBPA, which confers a shift in the density of MVBs[27].

Apart from this potential role of DGKα on the lipid composition of MVBs, it is conceivable that DGKα activity may affect the gradient of DAG at the synapse, this gradient is crucial for MTOC polarization in CTLs[17]. DGKα relocates to the PM upon cell activation and regulates the intensity of

signalling of DAG-controlled pathways in T lymphocytes[11], thus it is conceivable that DGKα may contribute to maintain a DAG gradient at the synapse. Loss of this gradient as a result of DGKα downregulation could be responsible for the defect in MVBs polarization and degranulation. However, our data showing that R59949 increases polarized secretion of exosomes rules out that the inhibition of polarized secretion in DGKα-interfered cells may be due to the absence of DGKα kinase activity, that would otherwise control a DAG gradient at the PM. Our results describing an increment in exosome secretion by treatment with R59949 are in apparent contradiction with the studies by Quann et al.[17], showing that DGK kinase activity is required to maintain a stable DAG gradient. Treatment of CTLs with R59949 induced a defect in the persistence of both MTOC polarization and the secretion of cytolytic factors towards the synapse and CTL-mediated killing[17]. The divergence may be due to the fact that mouse CTLs, instead of human cell lines, were used in that study[17]; and no evaluation of the secretion of exosomes and their contribution to apoptosis was performed. In addition, in DGKα–overexpressing cells the secretion of exosomes is reduced, and there are few $CD63^+/LBPA^+$ vesicles per cell. However, the MVBs are transported, dock, and fuse normally with the PM in cells overexpressing DGKα. Thus, the inhibition of the formation of mature MVBs appears to be the limiting step in secretory traffic of exosomes, at least in cells overexpressing DGKα. Since GFP-DGKα translocates to the PM, it is conceivable that the gradient of DAG at the synapse that may control MVBs polarization[17] is maintained in these cells. In contrast, in DGKα-interfered cells the defective polarization of MVBs would constitute a different, limiting step for exosome secretion. Experiments involving the use of "caged" dioctanoylglycerol (DOG)[17] photoactivable at different locations (synapse, MVBs), and the expression of DAG sensors such as C1 domains of PKCθ fused to GFP[28,25] may help to evaluate spatio-temporal changes of DAG levels, both in DGKα-overexpressing and DGKα-interfered cells, and to study the consequences of these changes on traffic of MVBs and exosome secretion.

Taken together, our data support the idea that the combination of positive signals triggered by receptor stimulation and a fine-tuning effect of a negative regulator, i.e. the kinase activity of DGKα, control the secretory vesicle pathway that is responsible of the secretion of exosomes. The negative effect of DGKα kinase activity on traffic was exerted at the stage of formation of mature MVBs. In addition, a

non-kinase function of DGKα is necessary for polarization of MVBs and exosome secretion. These inferences may conciliate the DGKα interference data with the fact that R59949 kinase inhibitor enhances polarized secretion and rescues the negative effect of DGKα overexpression on exosome secretion. Thus, DGKα appears to coordinate both positive and negative signals that are exerted at two different stages of the traffic of MVBs; the balance of these signals seems to be crucial for exosome secretion.

MATERIAL AND METHODS

Cell cultures

J-HM1-2.2 cells expressing human muscarinic type 1 receptor (HM1R) have been described [29]; these cells stimulated with agonist carbachol have been widely used as an appropriate model to induce full activation signals [11] and AICD [13]. Raji B cell line was from ATCC.

Antibodies and reagents

The anti-DGKα antibody (Ab) for WB and immunofluorescence was from Abnova (Taiwan). Anti-Fas Ligand (CD95L) NOK-1 mAb, Lamp-1 (clone 25), anti-CD3 (UCHT1) and anti-Fas Ligand G247-4 for immunofluorescence were obtained from BD Biosciences and Santa-Cruz Biotechnology. Rabbit polyclonal anti-Fas Ligand (CD95L) Q-20 for Western blot (WB) was from Santa Cruz Biotechnology. Anti-CD63 (clone NKI-C-3) was from Oncogene. Anti-Golgi 58K protein (clone 58K-9) was from SIGMA. Anti-lysobisphosphatidic acid (LBPA) Ab 6C4 was a kind gift from Dr. J. Gruenberg. All horseradish peroxidase-coupled secondary antibodies were from Dako. Carbachol (CCh) was from SIGMA. The DGK inhibitor II (R59949) was purchased from Calbiochem. This inhibitor is specific for the type I DGK isotypes (as DGKα) but does not inhibit DGKζ[10,21](the other DGK isotype expressed in T lymphocytes[30]). Alexa Fluor-coupled secondary antibodies were from Invitrogen. Staphylococcal Enterotoxin E (SEE) was from Toxin Technology, Inc (USA). Cell tracker blue (CMAC) was from Invitrogen.

Expression vectors, siRNA interference vectors and transfection assays

The plasmids pEFbos-GFP, pEFGFP-DGKα, pEFGFP-DGKζ have been described [8,11,30]. pEFGFP-C1bosCD63 and pECFP-C1CD63 were a generous gift from Dr. G. Griffiths. pDsRed2-CD63 was prepared by subcloning cDNA corresponding to human CD63 from pEFGFP-C1bosCD63 into pDsRed2-C1 vector (BD Biosciences). Expression vectors for GFP-VPS4wt and GFP-VPS4EQ mutant were a gift from Dr. P. Whitley [31]. siRNAs expression was achieved by using pSUPER RNAi System (pSR-GFP bicistronic or pSuper plasmids) (Oligoengine). One sequence of human DGKα isoform was selected to generate 64 bp double-strand DNA oligonucleotides encompassing the 19-nucleotide interfering sequence 5'-GCCAGAAGACCATGGATGA-3' and a hairpin-forming

sequence, which were cloned in these plasmids. Equivalent sequence 5'-ACACAAGACCACAGATGAT-3' (mouse DGKα) or 5'-CTATGTGACTGAGATCGCA-3' (human DGKζ) isoform were used in negative control plasmids. For transfection experiments, cells were transiently transfected with 20-30 μg of the plasmids as described [32]. Expression vectors for DGKs or siRNAs vectors were cotransfected in Jurkat cells in molar excess (3:1) to exosome reporters (GFP-CD63).

Isolation of exosomes

The exosomes produced by equal number of cells for each experimental condition were isolated from the cell culture supernatants as previously described [6,7]. Using these standard protocols, culture supernatants of $20x10^6$ cells were centrifuged at low speed in sequential steps and then clarified to eliminate cells and cell debris. To obtain the exosomes from cells expressing the exosome reporters GFP-CD81, GFP-CD63 and DsRed2-CD63 a similar protocol was performed, although $1x10^6$ effector cells (Jurkat) were used. For the secretion of exosomes in immune synapse experiments, expression vectors for DGKs or siRNAs vectors were cotransfected in Jurkat cells in molar excess (3:1) to exosome reporter vectors (i.e. GFP-CD63), and the formation of synapses with Raji cells in the absence (control) or presence of superantigen (SEE) was performed 2-3 days after transfection as described below. The exosomes were recovered by ultracentrifugation (100.000xg for 12 h) as described [6], and resuspended in 50 μl of RIPA lysis buffer, or directly quantified by flow cytometry (see below). We usually loaded 25 μl of this lysate per lane for WB analysis. We commonly obtained between 50-150 μg of protein in the 100000xg pellet from $20x10^6$ CCh-stimulated cells. In the experiments that involved the isolation of exosomes and WB, each lane of the blot contained the total protein that was recovered in the culture medium from the same number of cells, untreated or treated with stimuli in the presence or in the absence of DGK inhibitor. The lysates of the cells recovered after the first step of the protocol for exosome isolation were run in parallel to the exosomes, to internally normalise WBs by viable cell number at the end of the culture period for exosome secretion, but also to normalise transfection efficiency of the XFP-CD63 reporter. Alternatively, the number of exosomes in the clarified culture supernatants was quantified by flow

cytometry, using a constant acquisition period (5 min) and calibration fluorescent beads (50 and 100 nm beads, from SIGMA). Forward and side scatter light detectors together with gating regions, were set up to detect properly the calibration beads, and the absolute number of gated events equal to number of exosomes was represented using dot plot (forward versus side scatter) analysis. In parallel, samples corresponding to complete medium including the different reagents, but in the absence of cells, were analysed, and these dot plots registered a constant number of events; thus events above this background were considered as specific, cell-produced vesicles.

Western blot analysis

Cells and exosomes were lysed for 10 min in RIPA buffer containing protease inhibitors, and the proteins separated by SDS-PAGE under reducing conditions and transferred to Hybond™ ECL™ membranes (GE Healthcare). For CD63 detection, proteins were separated under non-reducing conditions as described [8]. After incubation with the appropriate primary antibody, the blots were developed with HRP-conjugated secondary antibodies using enhanced chemiluminescence (ECL) reagents and following standard protocols.

Cell fractionation

J-HM1-2.2 cells were disrupted in 2 ml of an iso-osmotic homogenization buffer [2] and the homogenate was fractionated on a discontinuous Percoll (Amersham Pharmacia) gradient as described [2,8]. The subcellular fractions from the same number of control and stimulated cells were analysed in parallel for the presence of CD63, FasL, DGKα and Lamp-1 proteins by WB. Lamp-1 was used as an appropriate, internal loading control. Density was calibrated using density marker beads (Amersham Pharmacia).

Electron microscopy

JHM1-2.2 cells were fixed for 20 min at RT in 2% PFA/1.5% glutaraldehyde in 0.1 M sodium cacodylate, pH 7.4. Cells were washed twice in 0.1 M sodium cacodylate and were spun into a tight pellet for osmication with 1.5% potassium ferricyanide, 1% osmium for 1 h at 4º C. The cell pellet was washed several times with 0.1 M sodium cacodylate and incubated with 1% tannic acid in 0.05 M sodium cacodylate for 45 min at room temperature. The cell pellet was rinsed in 1% sodium sulphate

in 0.05 M sodium cacodylate for 5 min and with dH_2O for 3 min. The cell pellet was dehydrated stepwise in ethanol (70%-90%-absolute ethanol). Ethanol was removed and propylene oxide was added for 2 x10 min and the cell pellet was embedded in 1:1 mixture of epon and propylene oxide. 60-70 nm ultra-thin sections were cut on an ultramicrotome, collected onto grids and examined with a Philips EM420 transmission electron microscope.

Immunofluorescence analysis

For fluorescence analysis of living J-HM1-2.2 cells expressing the different constructions, cells were attached to glass-bottom 35 mm culture dishes (Mat-Tek) using fibronectin at 24-48 h post-transfection, and stimulated in culture medium without phenol red at 37 ºC [32]. In some experiments, immune synapses between GFP-CD63 expressing Jurkat cells and Raji B cells pulsed with superantigen SEE and labelled with CMAC were performed as previously described [24]. Subsequently, epifluorescence images were taken with a Nikon Eclipse TE2000S microscope equipped with a DS-5M digital camera and a Plan Apo VC 60x NA 1.4. objective. Time lapse analysis was performed in living cells using ACT2-U software or NIS-AR software (NIKON). After the culture period, samples were either cell-surface stained or fixed and stained as described [32] with primary Abs (anti-CD63, anti-LBPA, anti-DGKα, anti-FasL) and appropriate secondary Alexa Fluor-conjugated Abs (Invitrogen). Confocal microscopy was performed using a Bio-Rad Radiance 2100 scan head mounted on a Nikon ECLIPSE TE 2000U microscope and using 60x NA 1.4 PlanApo objective. No labelling was observed when using the secondary Abs alone. Z-axis projection (maximun intensity) and merged images for colocalization experiments were performed using ImageJ software. For quantification, digital images were analysed using EasiVision SIS image analysis software (Soft Imaging Software, Munster, Germany) and ImageJ software (Rasband, W.S., ImageJ, National Institutes of Health, Bethesda, Maryland, USA, http://rsb.info.nih.gov/ij/, 1997-2004). Experimental significance of the results obtained at the single cell level was achieved by analysing a minimal number of 60 cells (unless otherwise indicated) from different microscope fields, and a minimal number of 3 independent experiments. Results were expressed as average minus/plus standard deviation (SD), and correspond to the means of the separate experiments, and not to the pooled cells measured together. ANOVA

analysis was perfomed for statistical significance of all the results. Trajectories of vesicles in videos were plotted by using NIS-AR software (NIKON). Epifluorescence image improvement was achieved by using deconvolution software (Huyghens, SVI).

Flow cytometry

After the indicated culture periods, cells were fixed and intracellularly stained with no Ab (negative controls) or primary Abs (anti-CD63, anti-LBPA, anti-FasL) and appropriate secondary, PE or FITC-conjugated Abs (Becton Dickinson). A minimal number of 10000 cells were analysed for FL-1 or FL-2 fluorescence by using FACSCAN flow cytometer (Becton Dickinson). For the experiments involving analysis of cell surface CD63 on Jurkat cells after synapse formation, Raji cells preloaded with CMAC were excluded from the flow cytometry analysis by electronic gating of CMAC-negative cells, and comparison of the CD63 red fluorescence on both Jurkat GFP- and GFP+ cells was performed using a FACS-Vantage flow cytometer equipped with an UV excitation laser.

ACKNOWLEDGEMENTS

We thank Dr. G. Griffiths (University of Oxford, UK), Dr. P. Whitley (University of Bath, UK), and Dr. Sánchez-Madrid (Hospital de la Princesa, Madrid) to generously provide us some of the plasmids we used in this study. We thank Alba García and Ana Sánchez for excellent technical support.

REFERENCES

1. Stoorvogel, W, Kleijmeer, MJ, Geuze, HJ and Raposo, G, (2002) The biogenesis and functions of exosomes. Traffic 3: 321-30.
2. Bossi, G and Griffiths, GM, (1999) Degranulation plays an essential part in regulating cell surface expression of Fas ligand in T cells and natural killer cells. Nat Med 5: 90-6.
3. Nagata, S, (1997) Apoptosis by death factor. Cell 88: 355-365.
4. Zuccato, E, Blott, EJ, Holt, O, Sigismund, S, Shaw, M, Bossi, G et al., (2007) Sorting of Fas ligand to secretory lysosomes is regulated by mono-ubiquitylation and phosphorylation. J Cell Sci 120: 191-9.
5. Monleon, I, Martinez-Lorenzo, MJ, Monteagudo, L, Lasierra, P, Taules, M, Iturralde, M et al., (2001) Differential secretion of Fas ligand- or APO2 ligand/TNF-related apoptosis-inducing ligand-carrying microvesicles during activation-induced death of human T cells. J Immunol 167: 6736-44.
6. Martinez-Lorenzo, MJ, Anel, A, Gamen, S, Monle n, I, Lasierra, P, Larrad, L et al., (1999) Activated human T cells release bioactive Fas ligand and APO2 ligand in microvesicles. J Immunol 163: 1274-81.
7. Andreola, G, Rivoltini, L, Castelli, C, Huber, V, Perego, P, Deho, P et al., (2002) Induction of lymphocyte apoptosis by tumor cell secretion of FasL-bearing microvesicles. J Exp Med 195: 1303-16.
8. Alonso, R, Rodriguez, MC, Pindado, J, Merino, E, Merida, I and Izquierdo, M, (2005) Diacylglycerol kinase alpha regulates the secretion of lethal exosomes bearing Fas ligand during activation-induced cell death of T lymphocytes. J Biol Chem 280: 28439-28450.
9. Kayagaki, N, Kawasaki, A, Ebata, T, Ohmoto, H, Ikeda, S, Inoue, S et al., (1995) Metalloproteinase-mediated release of human Fas ligand. J Exp Med 182: 1777-83.
10. Topham, MK and Prescott, SM, (1999) Mammalian diacylglycerol kinases, a family of lipid kinases with signaling functions. J Biol Chem 274: 11447-50.
11. Sanjuan, MA, Jones, DR, Izquierdo, M and Merida, I, (2001) Role of diacylglycerol kinase alpha in the attenuation of receptor signaling. J Cell Biol 153: 207-20.
12. Strasser, A, (1995) Death of a T cell. Nature 373: 385-386.
13. Izquierdo, M, Ruiz-Ruiz, MC and López-Rivas, A, (1996) Stimulation of the PtdIns turnover is a key event for Fas-dependent, activation-induced apoptosis in human T lymphocytes. J. Immunol. 157: 21-28.
14. Roth, MG, (1999) Lipid regulators of membrane traffic through the Golgi complex. Trends Cell Biol 9: 174-9.
15. Baron, CL and Malhotra, V, (2002) Role of diacylglycerol in PKD recruitment to the TGN and protein transport to the plasma membrane. Science 295: 325-8.
16. Sprong, H, van der Sluijs, P and van Meer, G, (2001) How proteins move lipids and lipids move proteins. Nat Rev Mol Cell Biol 2: 504-13.
17. Quann, EJ, Merino, E, Furuta, T and Huse, M, (2009) Localized diacylglycerol drives the polarization of the microtubule-organizing center in T cells. Nat Immunol 10: 627-35.
18. Vanlandingham, PA and Ceresa, BP, (2009) Rab7 regulates late endocytic trafficking downstream of multivesicular body biogenesis and cargo sequestration. J Biol Chem 284: 12110-24.
19. Clark, RH, Stinchcombe, JC, Day, A, Blott, E, Booth, S, Bossi, G et al., (2003) Adaptor protein 3-dependent microtubule-mediated movement of lytic granules to the immunological synapse. Nat Immunol 4: 1111-20. Epub 2003 Oct 19.
20. Alonso, R, Mazzeo, C, Merida, I and Izquierdo, M, (2007) A new role of diacylglycerol kinase alpha on the secretion of lethal exosomes bearing Fas ligand during activation-induced cell death of T lymphocytes. Biochimie 89: 213-21.
21. Jiang, Y, Sakane, F, Kanoh, H and Walsh, JP, (2000) Selectivity of the diacylglycerol kinase inhibitor 3-[2-(4-[bis-(4-fluorophenyl)methylene]-1-piperidinyl)ethyl]-2, 3-dihydro-2-thioxo-4(1H)quinazolinone (R59949) among diacylglycerol kinase subtypes. Biochem Pharmacol 59: 763-72.

22. Bishop, N and Woodman, P, (2000) ATPase-defective mammalian VPS4 localizes to aberrant endosomes and impairs cholesterol trafficking. Mol Biol Cell 11: 227-39.
23. Fujita, H, Yamanaka, M, Imamura, K, Tanaka, Y, Nara, A, Yoshimori, T et al., (2003) A dominant negative form of the AAA ATPase SKD1/VPS4 impairs membrane trafficking out of endosomal/lysosomal compartments: class E vps phenotype in mammalian cells. J Cell Sci 116: 401-14.
24. Montoya, MC, Sancho, D, Bonello, G, Collette, Y, Langlet, C, He, HT et al., (2002) Role of ICAM-3 in the initial interaction of T lymphocytes and APCs. Nat Immunol 3: 159-68.
25. Sato, M, Ueda, Y and Umezawa, Y, (2006) Imaging diacylglycerol dynamics at organelle membranes. Nat Methods 3: 797-9.
26. Matsuo, H, Chevallier, J, Mayran, N, Le Blanc, I, Ferguson, C, Faure, J et al., (2004) Role of LBPA and Alix in multivesicular liposome formation and endosome organization. Science 303: 531-4.
27. Kobayashi, T, Beuchat, MH, Chevallier, J, Makino, A, Mayran, N, Escola, JM et al., (2002) Separation and characterization of late endosomal membrane domains. J Biol Chem 277: 32157-64.
28. Carrasco, S and Merida, I, (2004) Diacylglycerol-dependent binding recruits PKCtheta and RasGRP1 C1 domains to specific subcellular localizations in living T lymphocytes. Mol Biol Cell 15: 2932-42.
29. Desai, DM, Newton, ME, Kadlecek, T and Weiss, A, (1990) Stimulation of the phosphatidylinositol pathway can induce T cell activation. Nature 348: 66-69.
30. Santos, T, Carrasco, S, Jones, DR, Merida, I and Eguinoa, A, (2002) Dynamics of diacylglycerol kinase zeta translocation in living T-cells. Study of the structural domain requirements for translocation and activity. J Biol Chem 277: 30300-9.
31. Whitley, P, Reaves, BJ, Hashimoto, M, Riley, AM, Potter, BV and Holman, GD, (2003) Identification of mammalian Vps24p as an effector of phosphatidylinositol 3,5-bisphosphate-dependent endosome compartmentalization. J Biol Chem 278: 38786-95.
32. Jambrina, E, Alonso, R, Alcalde, M, Rodríguez, MC, Serrano, A, Martínez-A., C et al., (2003) Calcium influx through receptor-operated channel induces mitochondria-triggered paraptotic cell death. J. Biol.Chem. 278: 14134-14145.
33. Kobayashi, T, Stang, E, Fang, KS, de Moerloose, P, Parton, RG and Gruenberg, J, (1998) A lipid associated with the antiphospholipid syndrome regulates endosome structure and function. Nature 392: 193-7.
34. Babst, M, (2005) A protein's final ESCRT. Traffic 6: 2-9.
35. Babst, M, Wendland, B, Estepa, EJ and Emr, SD, (1998) The Vps4p AAA ATPase regulates membrane association of a Vps protein complex required for normal endosome function. Embo J 17: 2982-93.

FIGURE LEGENDS

Fig. 1. Cellular stimulation induces the formation of mature MVBs. A) Upper panel, J-HM1-2.2 cells were stimulated with CCh for 6 h and then were imaged by confocal microscopy using antibodies specific for CD63, FasL, and LBPA. Lamp-1 is mostly present on the limiting membrane of MVBs, whereas CD63, and particularly LBPA, are abundant in the ILVs [27] and therefore label mature MVBs. LBPA is a phospholipid that participates in the maturation of MVBs [33] and constitutes a bona fide marker for ILVs of mature MVBs [33]. Z- axis projections for each antigen corresponding to representative cells from 3 independent experiments are represented. Lower panel, quantitative analysis of vesicles. Vesicle numbers were recorded from at least 20 cells per group, chosen randomly as indicated in Material and Methods. Results represent average number of vesicles/cell $\pm$ SD of 3 independent experiments. B) J-HM1-2.2 cells transfected with CFP-CD63 were stimulated with CCh (for 6 and 16 h), and mature MVBs were visualised with anti-LBPA antibody (red) as indicated in Material and Methods. Cells were imaged by confocal microscopy and representative (n=3 independent experiments), single optical sections (0.4 μm thick) and merged images (coincident labelling appearing pink) are shown in the right side. In the left side, Z-projection images of LBPA and CFP-CD63 are shown.

Fig. 2. Cellular stimulation induces the relocalisation of Fas ligand and DGKα to subcellular fractions containing MVBs. Cellular fractionation by density gradient of the homogenates from equal numbers of J-HM1-2.2 cells, stimulated or not with CCh (6 hours), was performed as indicated in Material and Methods, and the Percoll fractions were analysed for CD63, DGKα, and FasL by WB. The blot was reprobed with anti Lamp-1 Ab as a loading control. Data are representative of the results obtained in 3 different experiments.

Fig. 3. Inhibition of DGKα kinase activity increases the number of MVBs and the secretion of exosomes. (A) The secretion of exosomes was induced by treatment of J-HM1-2.2 cells with CCh during 10 h, preincubated or not with R59949 (10 μM). In the upper row, the dot plots correspond to the events recorded – the number of events is included inside each plot - in the cell culture supernatants from cells treated as indicated, whereas the lower row plots register the events from complete medium treated with the different reagents but in the absence of cells. The lower row dot plots registered a constant number of

events; thus events above this background should be considered as specific, cell-produced vesicles. In the right-hand side, dot plots corresponding to 50 nm and 100 nm latex beads analysed in parallel are included as a reference. (B) WB with anti-CD63 of Percoll density gradient fractions from cells stimulated with CCh for 6 h, pretreated or not with R59949. Data are representative of the results obtained in 3 different experiments. The shift in the distribution of CD63 on the density gradient is compatible with changes in the lipid composition and the maturation of MVBs [27].

Fig. 4. DGKα is associated to CD63⁺ vesicles and exosomes. A) Cells expressing GFP-DGKα were stimulated with CCh for 6 h in the presence of R59949, stained with anti-CD63 (red) and cells were imaged by confocal microscopy; several representative, optical sections (0.4 μm thick) are shown. The right-hand panels show the merged images, with coincident labelling appearing yellow. B) Digital zoom (1.67x) of some images from one experiment similar to that described in panel A are shown. C) Cells were stimulated or not with CCh (50 and 500 μM) for 12 h in the presence or absence of R59949 (10 μM), and the secreted exosomes were analysed by WB for the presence of several exosome markers and endogenous DGKα. Results are representative of the data obtained in 3 different experiments.

Fig. 5. Expression of the reporters for MVBs/exosomes in living cells. A) J-HM1-2.2 cells expressing DsRed2-CD63 (upper panels) or GFP-CD63 (lower panels) were stimulated with CCh for 10 h in the presence or the absence of R59949 inhibitor (R59, 10 μM), and the isolated exosomes were analysed by WB with anti-CD63 to detect the chimerical CD63 molecules. Different exposures of the same blot are shown to visualize both the chimeras and the endogenous CD63. In the right side lanes of each blot, lysates from cells expressing or not the CD63 chimeras were run as a reference. B) Cells expressing GFP-CD63 were stimulated or not with CCh for 6 and 24 h in the presence or the absence of R59949, in order to visualize the formation and fate of MVBs in living cells. The CCh and R59949-induced increase in GFP-CD63 at the plasma membrane, was probably due to the fusion of the limiting membrane of GFP-CD63⁺ MVBs (See also Supplementary Material, videos 3 and 4). The epifluorescence images were improved by image deconvolution as indicated in Material and Methods, and are representative of the results obtained in more of 50 cells recorded per treatment in 4 independent experiments. The inset shows a 2X digital zoom of the indicated area.

Fig. 6. Expression of GFP-DGKα affects the formation of mature MVBs and the distribution of LBPA$^+$ vesicles, but does not inhibit the accumulation of CD63 at the plasma membrane. Jurkat cells expressing GFP-VPSwt, GFP-VPS4EQ mutant or GFP-DGKα, together with CFP-CD63, were stimulated with CCh to induce the formation and traffic of MVBs, and LBPA was stained as indicated in Material and Methods. The ESCRT (Endosomal Sorting Complex Required for Transport) machinery is involved in the formation of the intraluminal vesicles of MVBs and the AAA-ATPase vacuolar protein sorting VPS4 regulates the recycling of the ESCRT complexes [34]. The expression of a VPS4 ATPase-defective mutant, VPS4EQ, inhibits the inward budding at the limiting membrane of MVBs and the subsequent formation of ILVs [22,35]. These effects result in the formation of immature, large endosomes [22,23], and thus the expression of VPS4EQ mutant constitutes an appropriate control for aberrant MVBs maturation. A) Epifluorescence microscopy images (GFP-X, CFP-CD63, and LBPA, respectively) of control and CCh-stimulated (8 h) cells. In GFP-VPS4EQ-expressing cells the dispersion of LBPA$^+$ granules that was induced by CCh in GFP-VPS4EQ$^-$ cells or in cells expressing GFP-VPS4wt was inhibited, and the large LBPA$^+$ structures accumulated in the perinuclear area. B) Cells expressing GFP-DGKα (upper rows) or GFP-VPS4EQ (lower rows), together with CFP-CD63 were stimulated with CCh for the indicated times to visualize the accumulation of CFP-CD63 at the plasma membrane by fluorescence microscopy. CD63 cell surface labelling is a consequence of the transport, docking and fusion of MVBs with the plasma membrane (See also Fig. 5B, Supplementary Videos 3 and 4). C) The average number per cell and the mean diameter (±SD) of LBPA$^+$ vesicles were measured in cells from 3 independent experiments similar to that described in panel A (in a total of 11 control, untransfected cells, 8 GFP-DGKα$^+$ cells, and 19 GFP-VPS4EQ$^+$ cells) after 6 h of CCh stimulation. In a significant fraction (40-50%, n=20 cells) of GFP-DGKα-expressing cells the number of LBPA$^+$ vesicles was lower to that found in GFP-DGKα$^-$ cells stimulated with CCh (Suppl. Fig. S5, panel A, third row). In approximately 20% of GFP-DGKα$^+$ cells, the LBPA$^+$ structures were condensed in some areas but not dispersed throughout the cytosol (Suppl. Fig. S5, panel A, lower row), as observed in GFP-VPS4EQ$^+$ cells (Suppl. Fig. S5, panel A, second row). See also Supplementary Fig. S5, panel C.

Fig. 7. Modulation of DGKα pathway controls the polarized secretion of exosomes. Jurkat cells coexpressing GFP-DGKα or GFP, together with GFP-CD63 were mixed with Raji cells, pulsed or not with SEE, to induce the formation of synapse and the secretion of exosomes. Upper panel: the amount of exosomes produced by cells expressing similar amounts of GFP-CD63 (cell lysates, right side) at the end of the culture period was measured by WB with an antibody against CD63. Middle panel: Quantification of the secretion of exosomes in cells expressing GFP-DGKα in comparison to cells expressing GFP. Results summarize the data obtained from WB in 4 independent experiments and are represented as average (±SD) fold induction of exosome secretion. Lower panel: the effect on exosome secretion of the pretreatment with R59949 (10 μM) of cells expressing GFP (control), GFP-DGKα, or GFP-DGKζ was measured as indicated in the middle panel (n=3 independent experiments).

Fig. 8. Interference of DGKα inhibits polarized exosome secretion. Jurkat cells were cotransfected with interference plasmids for human DGKα, human DGKζ, or an irrelevant, mouse DGKα, together with reporter GFP-CD63, and were stimulated with Raji cells, pulsed or not (control) with SEE, to induce secretion of exosomes. Transfection efficiency of Jurkat cells in these experiments was around 50%, as assessed by flow cytometry. A) WB of Jurkat cells transfected with the interference plasmids before stimulation with Raji cells, showing the specificity of the interference with specific antibodies against DGKα and DGKζ. B) WB of the exosomes (upper panel) isolated from the cell culture supernatants of the interfered cells after synapse formation (12 h). In the right side, extracts of cells transfected with an empty vector and a GFP-CD63 vector were analysed as reference. The WB of the cells (lower panel) recovered after the culture period was performed in parallel to normalise by viable cell number at the end of the culture period and by transfection efficiency of the GFP-CD63 reporter**.** C) Summary of the results from 4 independent experiments similar to the one shown in panel B; results are represented as average (±SD) percent of SEE induction of exosome secretion.

Fig. 9. Interference of DGKα affects polarization and degranulation of MVBs at the immune synapse. Jurkat cells transfected with a GFP-containing, bicistronic interference plasmid for human DGKα were stimulated for 1 and 5 h with Raji cells previously pulsed with SEE and labelled with CMAC (blue), to induce synapse formation and the polarized traffic of MVBs. A) Upper panel:

Degranulation of MVBs at the synapse after 5 h was assessed by cell surface staining of endogenous CD63 (orange-red) and fluorescence microscopy. White arrowheads label the synaptic contact areas made by GFP^- Jurkat cells, whereas green arrowhead labels the synapse corresponding to a GFP^+ Jurkat cell. Images are representative of the results obtained in 4 different experiments. Lower panel: Degranulation induced by SEE was measured after 1 and 5 h, by analysing cell surface staining of CD63 in both GFP^+ ($DGK\alpha^-$) and GFP^-($DGK\alpha^+$) Jurkat cells by flow cytometry. The FACS profiles corresponding to the staining of Jurkat cells challenged with Raji without SEE are not shown for clarity, but the corresponding MFI (Mean Fluorescence Intensity) data are included (Control). B) Upper panel: Quantification of LBPA+ and CD63+ intracellular vesicles in Jurkat cells forming synapse with SEE-pulsed Raji cells during 5 hours. Middle panel: polarization of MVBs towards the synapse after 5 h was assessed by intracellular labelling of endogenous CD63 (orange-red). Interference with DGKα expression was tested by intracellular staining of endogenous DGKα (red). White arrowheads label synapses made by GFP^- $DGK\alpha^+$ Jurkat cells, whereas green arrowhead labels the synapse corresponding to a GFP^+ $DGK\alpha^-$ Jurkat cell. Images are representative of the results obtained in 4 different experiments. The insets shows a 2x digital zoom of the indicated areas. Lower panel: the graph summarizes the results of 4 independent experiments (at least 40 cells per condition were analysed) similar to the one described in the middle panel, and compares the percentage of cells with polarized MVBs after 1 and 5 h of stimulation, both in $DGK\alpha^+$ cells and $DGK\alpha^-$ cells. Cells with polarized MVBs were defined as those cells on which the majority of their MVBs located at a distance of the synapse lower than one quarter of the diameter of the cell. The interference on DGKα expression does not affect the interaction among T lymphocytes and the SEE-presenting cells, since the frequency of formation of Raji/Jurkat conjugates was not affected by DGKα interference (not shown).

LEGENDS FOR ONLINE SUPPLEMENTAL MATERIAL

Videos 1 and 2

J-HM1-2.2 cells expressing CFP-CD63 were either left untreated (Video 1) or stimulated with CCh for 24 h (Video 2). After this period, videos were captured at 8 frames per second and a frame size of

640x480 pixels using a Nikon DS-5M camera. The videos were edited using ImageJ and VirtualDub software. The final frame display rate is 6 frames per second. Blue represents the chimerical CFP-CD63 molecule.

Videos 3 and 4

J-HM1-2.2 cells expressing GFP-CD63 were stimulated with CCh for 3 h (Video 3) or 6 h (Video 4). Videos were captured and processed as previously indicated; green represents GFP-CD63. In video 3, the movement of a GFP-CD63$^+$ vesicle towards the plasma membrane and its disappearance in proximity to the membrane can be observed in the lower part of the cell located in the left side. This extinction event took place concomitantly to a transient increase in fluorescence at the docking site at the cell surface (Video 3), which may be due to the fusion of a GFP-CD63-containing vesicle with the PM. In video 4, the extinction of a ring-shaped, GFP-CD63-decorated vesicle can be observed in the right side of the cell.

Video 5

Raji B cells labelled with cell tracker blue (CMAC, blue) were pulsed with SEE for 30 min and synapses with Jurkat cells expressing GFP-CD63 were formed as indicated in Material and Methods. 4 hours after synapse formation, videos corresponding to GFP-CD63 were captured (7 frames per second) and a representative example out of 47 synapses recorded is shown. See also Supplementary Fig. S6 to visualize CMAC fluorescence corresponding to this experiment.

Video 6

Same as video 5, but the formation of a double synapse between one Jurkat cell and two Raji cells (CMAC, blue) was recorded from the beginning (10 frames per second). Simultaneous capture of GFP-CD63 and CMAC fluorescence was performed using NIS-AR software. Deconvolution of the GFP-CD63 fluorescence channel was performed as indicated in Material and Methods. A representative example out of 11 synapses recorded is shown.

Supplementary Fig. S1. J-HM1-2.2 cells were stimulated with CCh or not (Control) for the indicated times, stained with anti-CD63, anti-FasL, or anti-LBPA, and the fluorescence (Mean Fluorescence

Intensity, MFI) measured by flow cytometry. Negative samples (Neg) correspond to cells stained only with secondary antibody. In the inset from the middle panel, a WB of cell extracts developed with anti-FasL (Q-20 Ab) is shown.

Supplementary Fig. S2. Quantitation of LBPA+ CD63+ vesicles and statistical analysis of the results obtained in similar experiments to that represented in Fig. 1B was performed as described in Material and Methods, in cells stimulated or not (control) with CCH (6 and 16 h). Results are represented as average number (±SD) of vesicles per cell and summarize the results obtained in 4 independent experiments.

Supplementary Fig. S3. Electron microscopy of MVBs. J-HM1-2.2 cells were stimulated with CCh for 8 hours in the presence or the absence of R59949 and processed for electron microscopy as indicated in Material and Methods. Representative sections of the results obtained with at least 30 different cells are shown. Black arrowheads label vesicles resembling MVBs. Some enlarged areas (insets 1 to 4) showed the presence of electron-dense ILVs inside MVBs. KEY: n; nucleus; M; mitochondria; G; Golgi. Lower panel: the mean number (±SD) of MVBs per cell is represented. Quantitation was performed by counting vesicles on randomly chosen sections, and summarize the results from 4 different experiments.

Supplementary Fig. S4. Cells pretreated or not with R59949 (10 μM) were stimulated with CCh for 6 h. Left panel: confocal microscopy of cells after CD63 and LBPA labelling (Z-projections). Representative images of the results obtained in 3 independent experiments are shown. Right panels: quantitation of the number of $CD63^+$ and $LBPA^+$ vesicles. Results are represented as average numbers (± SD) of vesicles/cell from 40 cells analysed in 3 independent experiments. R59949 alone had no effect on the number of $CD63^+$ or $LBPA^+$ intracellular vesicles**.**

Supplementary Fig. S5. A) Cells were transfected with different GFP fusion constructs (GFP-VPS4wt, GFP-VPS4EQ and GFP-DGKα), stimulated with CCh (8 h) and stained with anti-LBPA, and imaged by confocal microscopy. Z-projection images of the GFP-containing construction and LBPA staining are

shown to visualize the effect of the different constructions on the subcellular distribution of LBPA. B) Cells expressing GFP-VPS4EQ mutant together with CFP-CD63, were stimulated for 8 h with CCh and stained with anti-LBPA (red) as indicated in Material and Methods. Cells were imaged by confocal microscopy and a representative, single optical section (0.4 μm thick) is shown in the upper row. The lower row shows the merged images, with coincident labelling appearing yellow, pink and sky blue, respectively. C) The vesicle diameter distribution analysis corresponding to the experiment summarized in Fig. 6C was performed as indicated in Material and Methods. The distribution is represented as a histogram of the average (±SD) vesicle number per cell versus the indicated vesicle diameter classes.

Supplementary Fig. S6. Raji B cells labelled with CMAC (R) were pulsed with SEE and synapses with Jurkat cells expressing GFP-CD63 (J) were formed as indicated in Material and Methods. Four hours after synapse formation, snapshots (transmittance plus CMAC, GFP-CD63) and videos (GFP-CD63, see Video 5 synapse) were recorded as indicated in Material and Methods. In the middle panel, the first frame corresponding to video 5 is shown, and one synapse area is seen at the upper left side of the Jurkat cell. In the right side panel, trajectories followed by GFP-CD63 vesicles from video 5 are plotted.

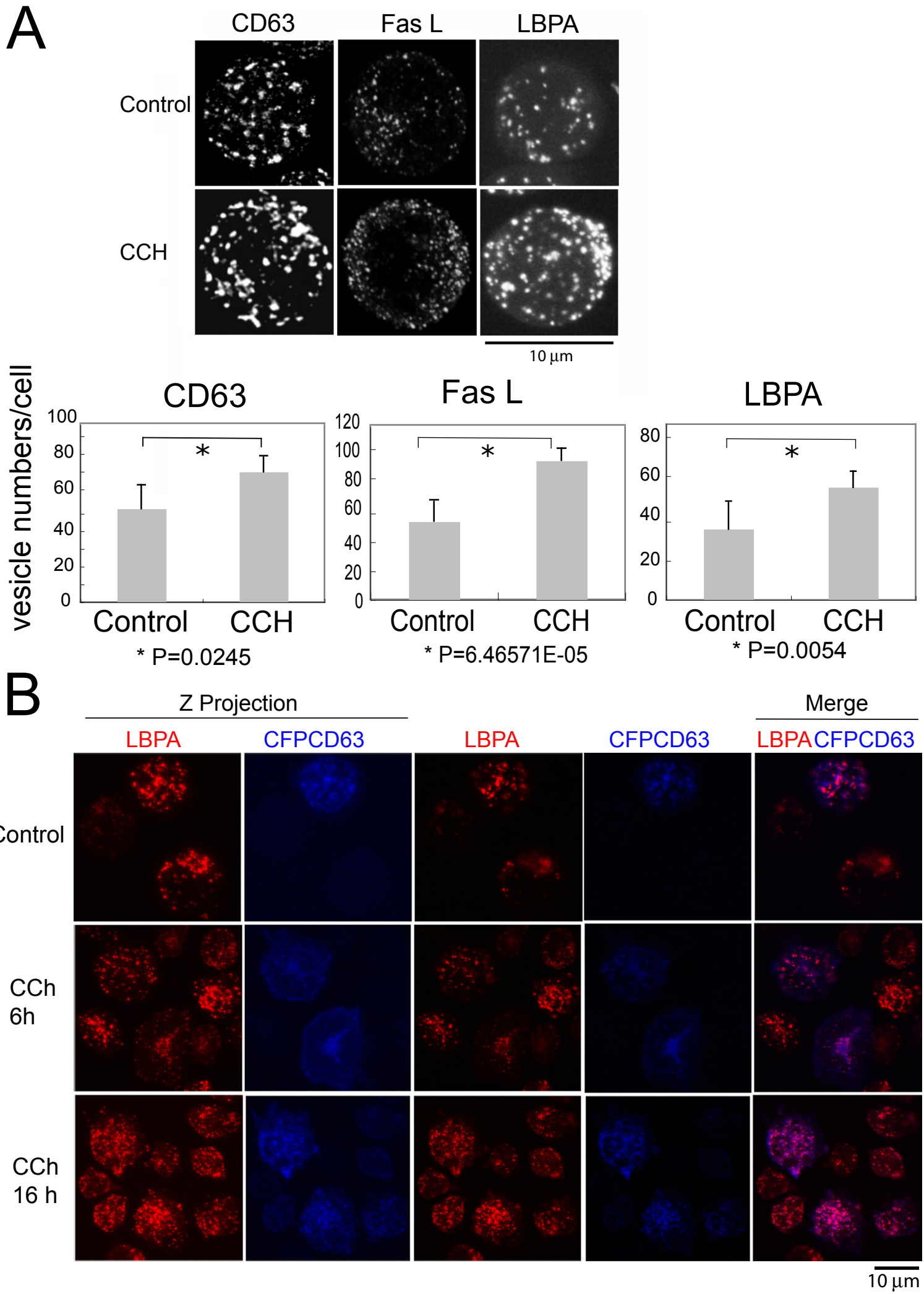

Fig. 1 Alonso et al

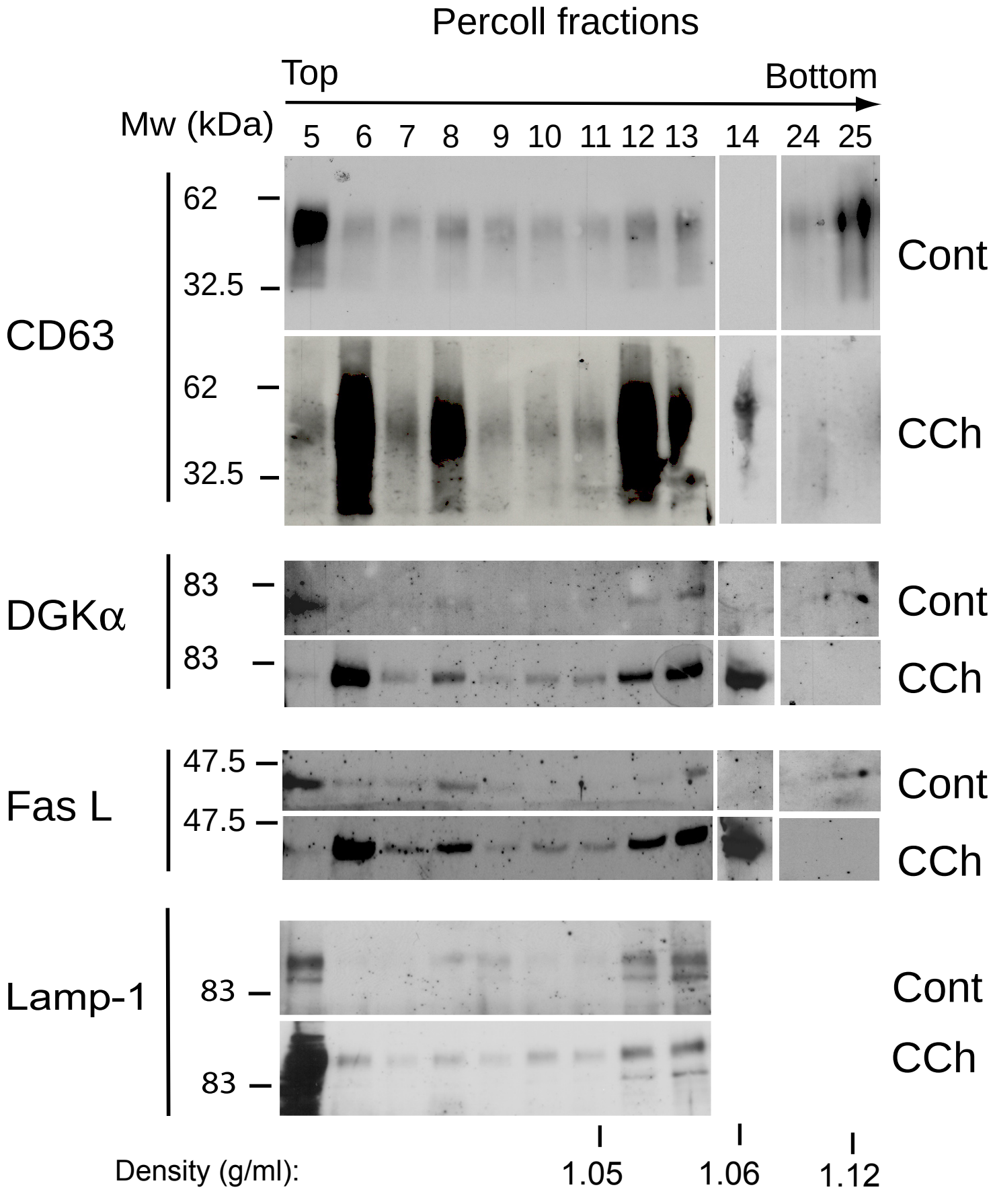

Fig. 2 Alonso et al

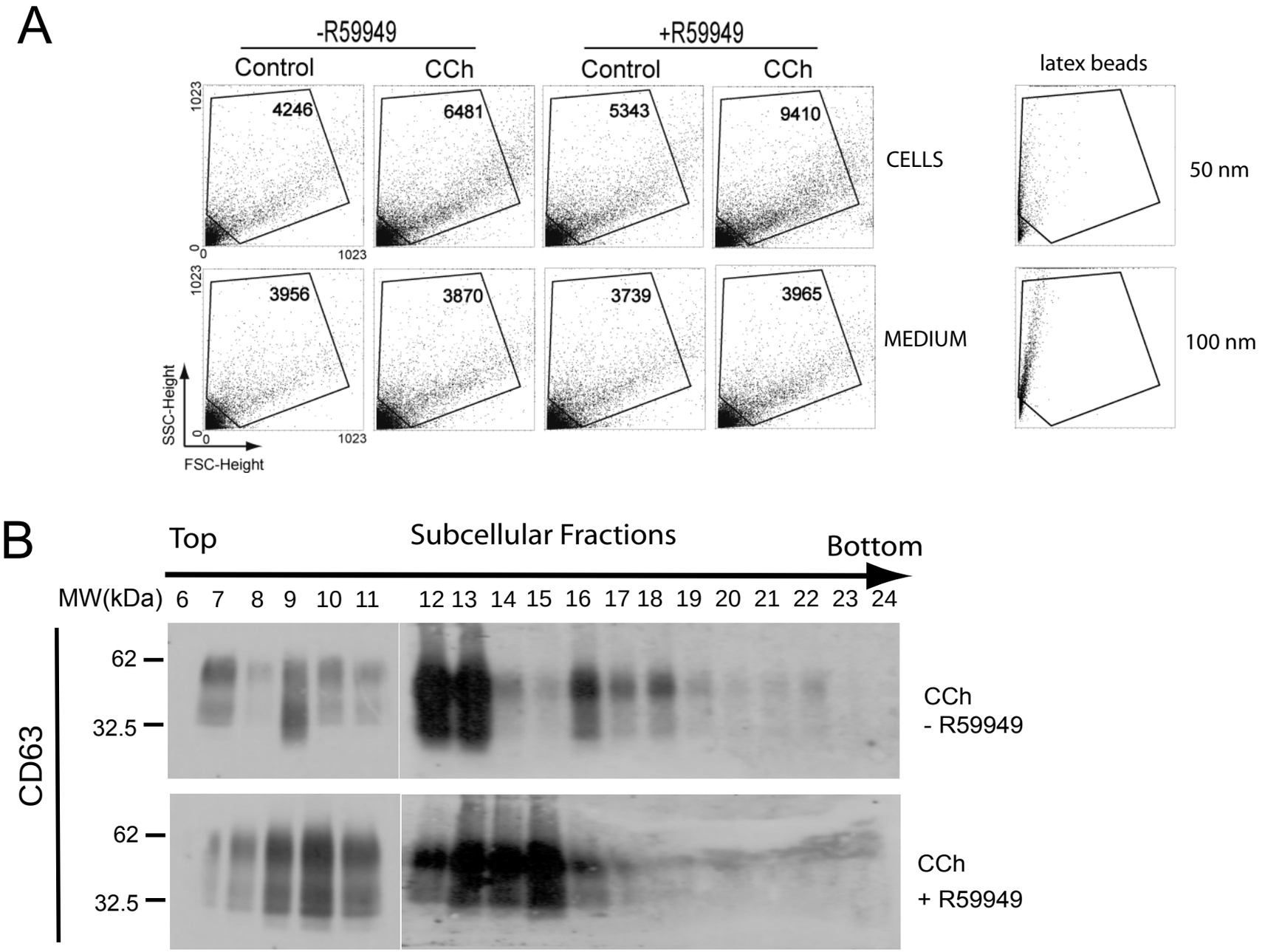

Fig. 3 Alonso et al.

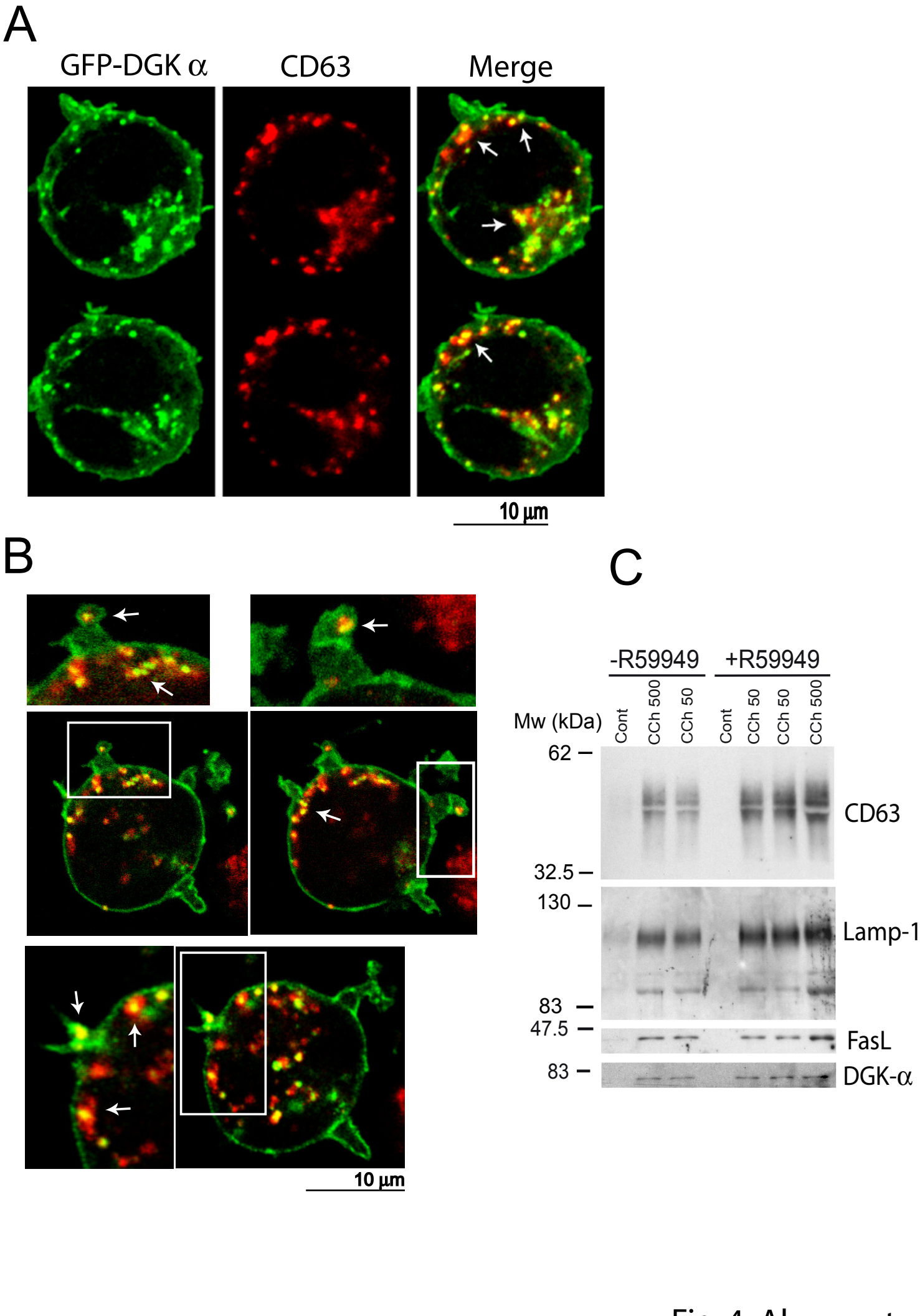

Fig. 4 Alonso et al

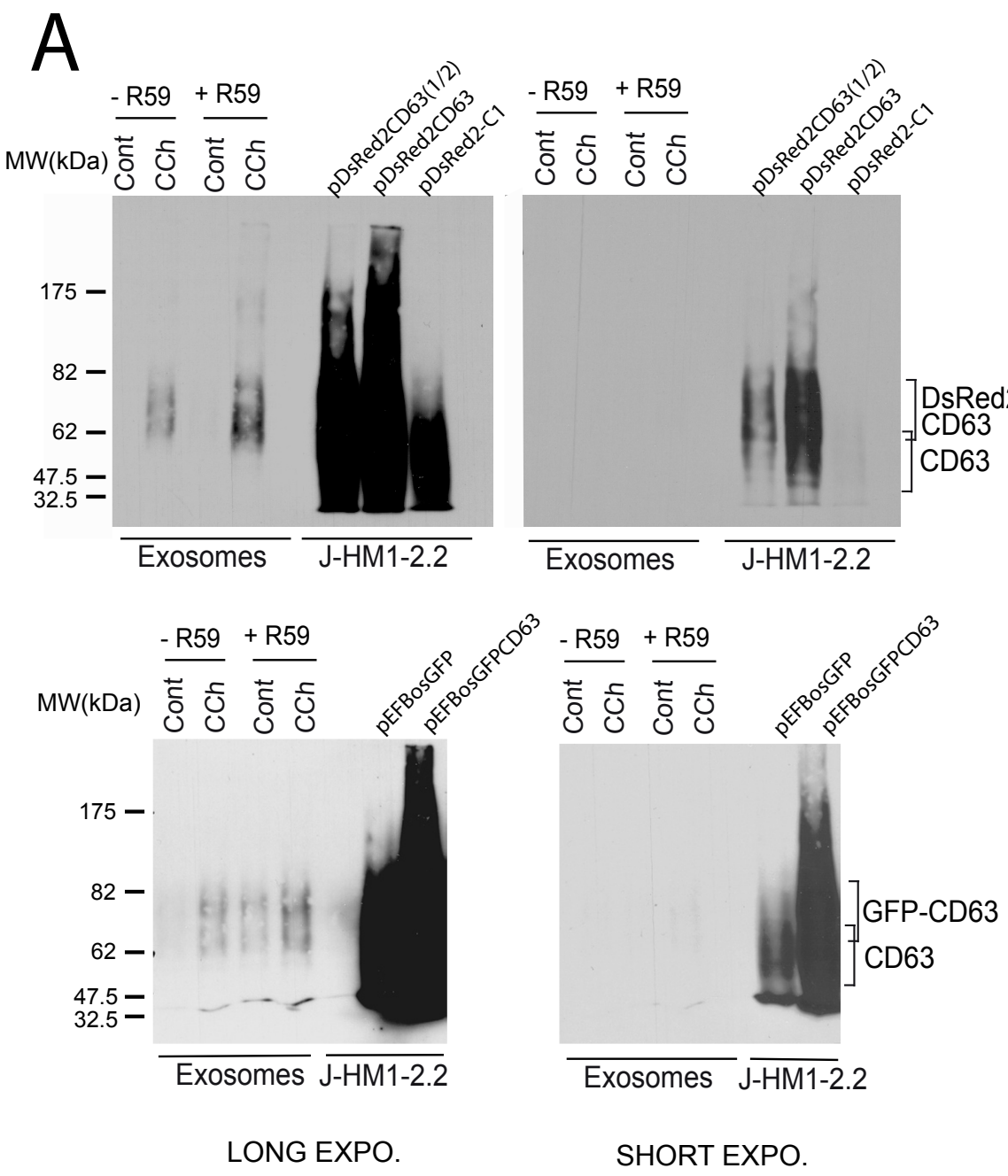

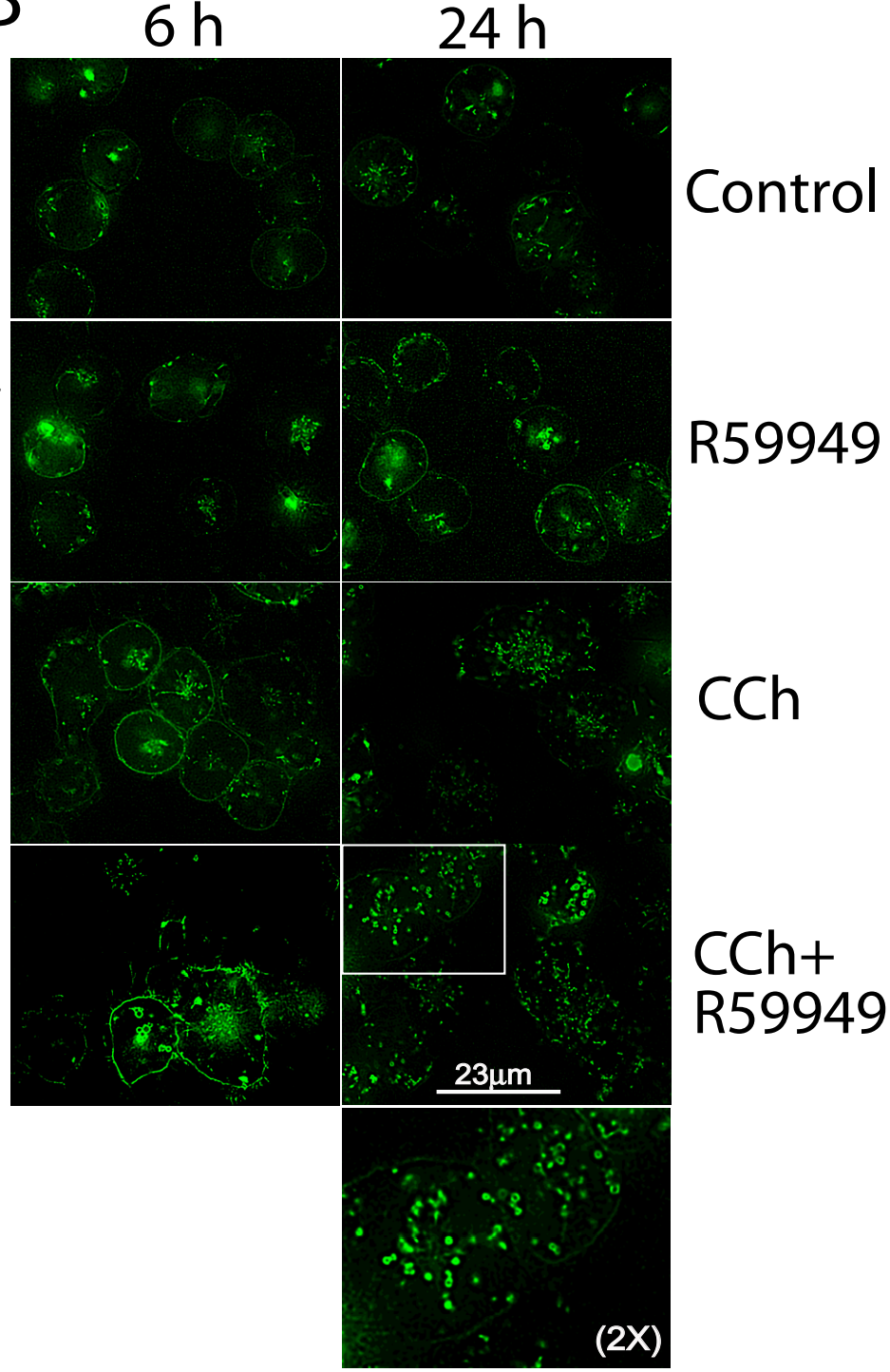

Fig. 5 Alonso et al.

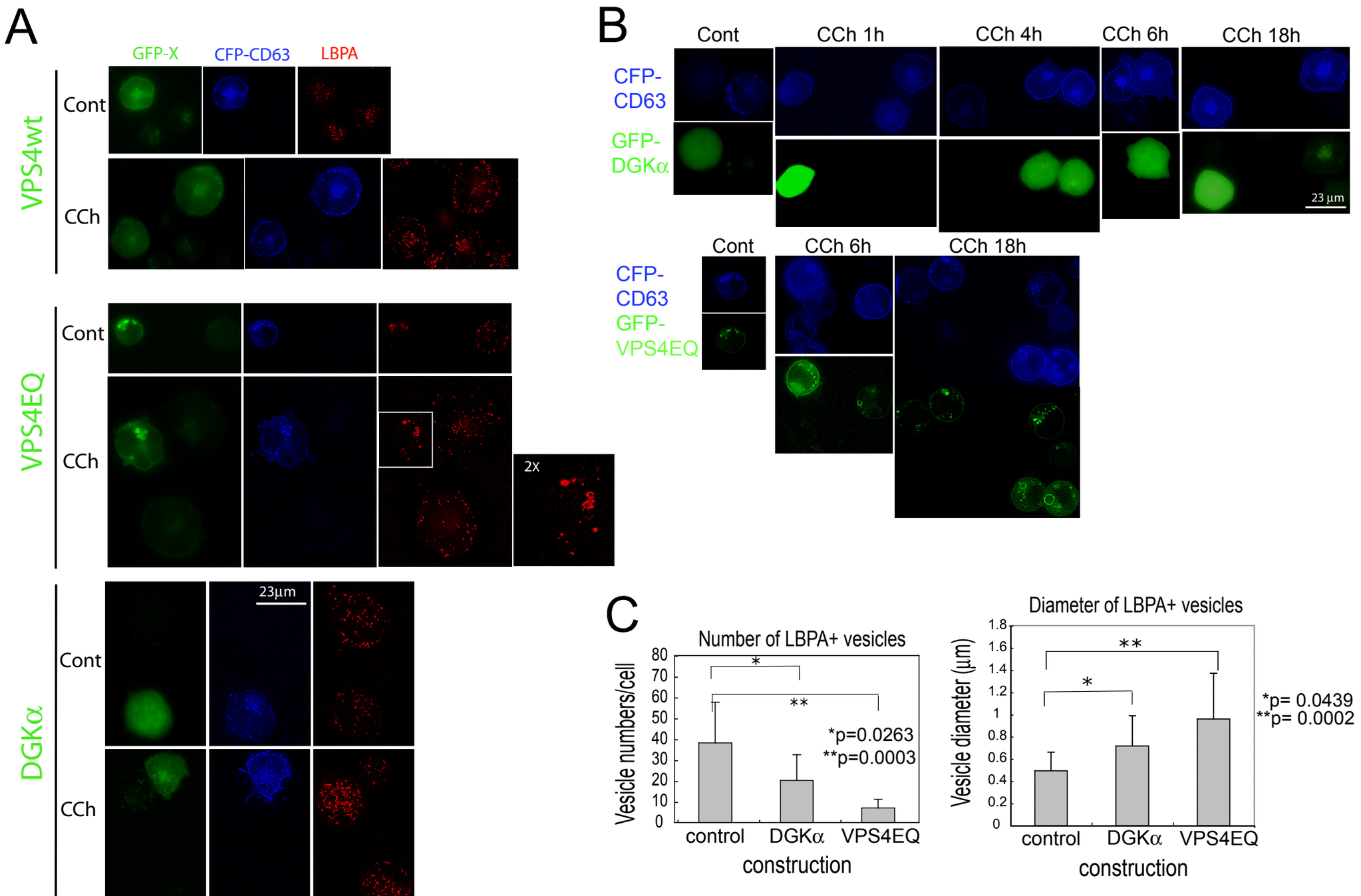

Fig. 6 Alonso et al.

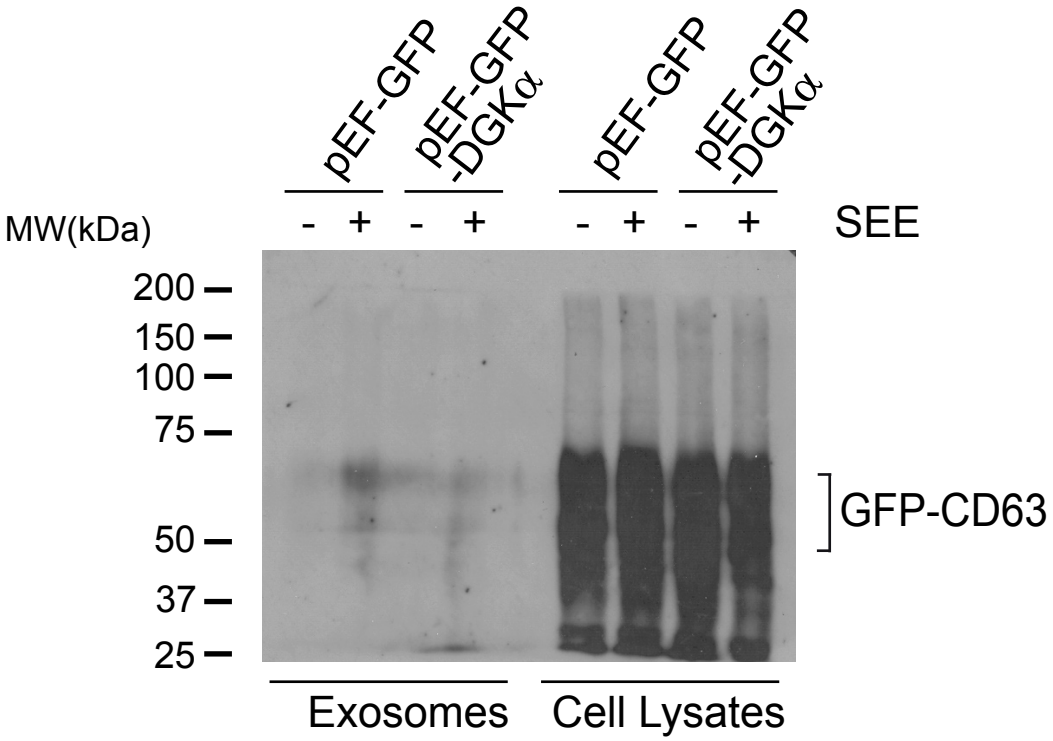

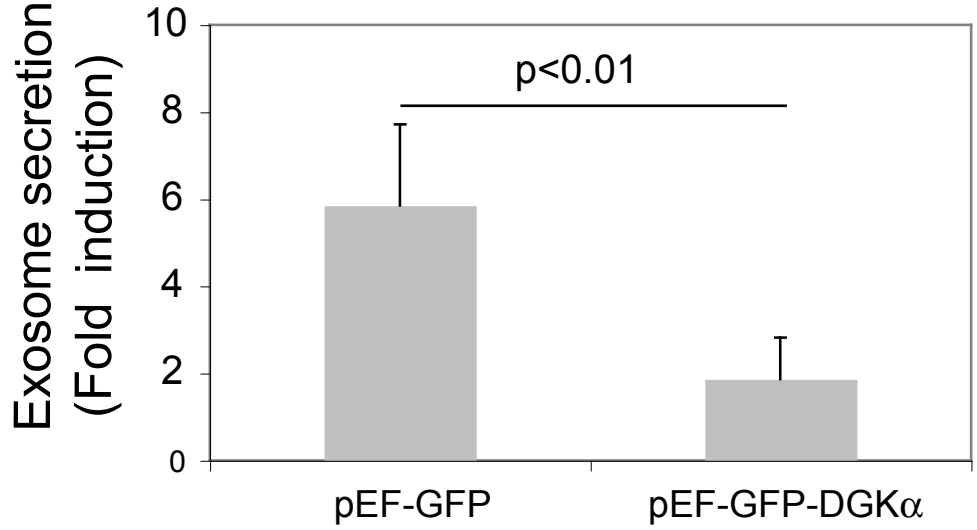

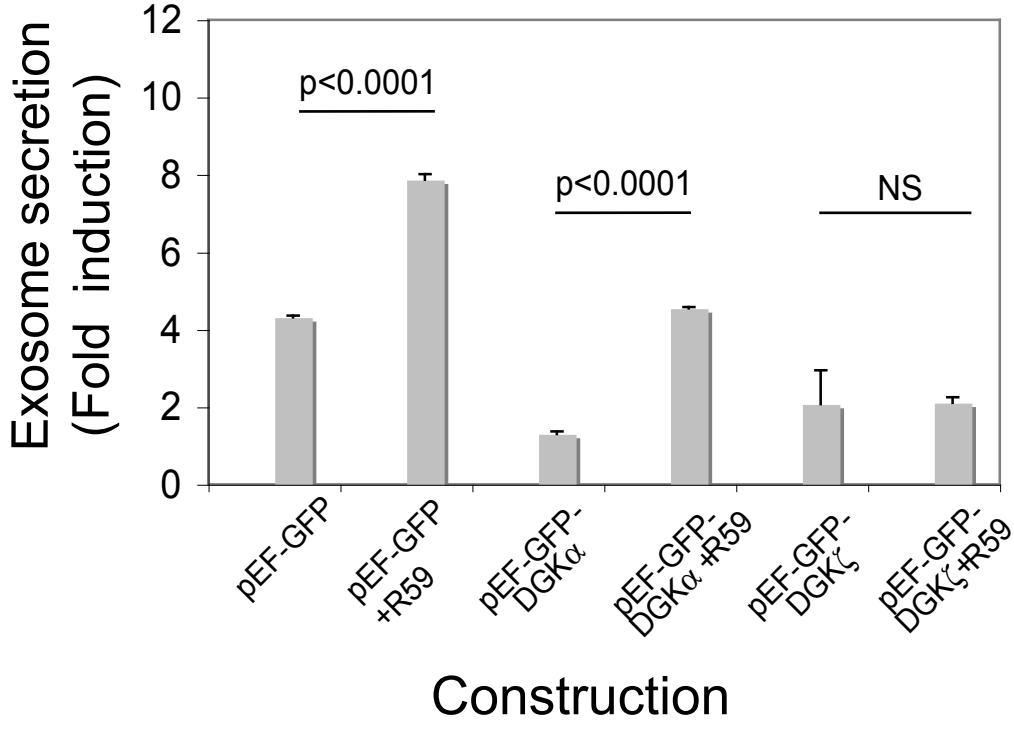

Fig. 7. Alonso et al.

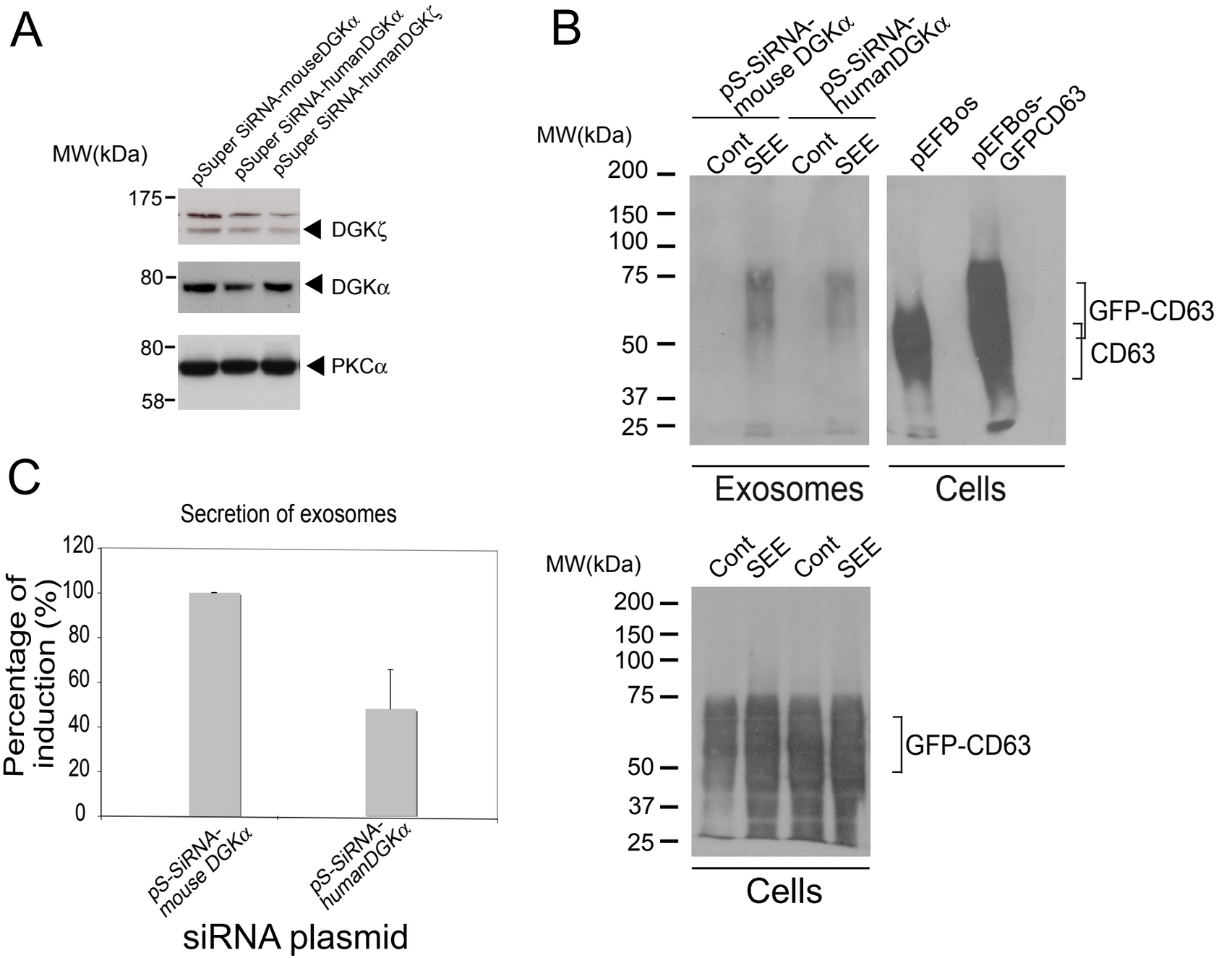

Fig.8. Alonso et al.

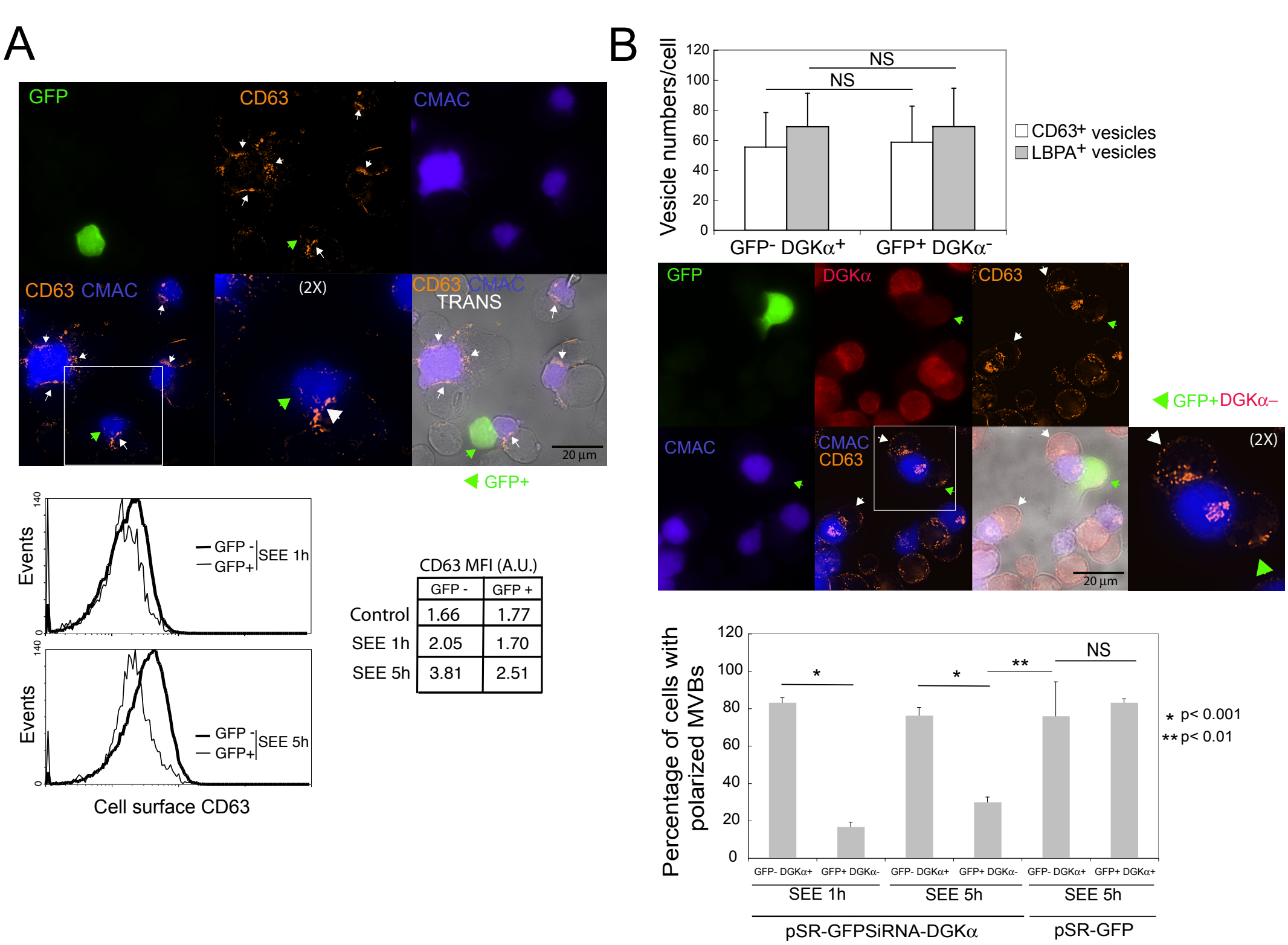

Fig. 9A. Alonso et al.